for which the required threshold η_2' can be computed as

$$\eta_2' = \mathrm{erfc}^{-1}(2\alpha_2)\sqrt{2}\sigma_{2n_e}. \quad (33)$$

To obtain an approximate threshold η_2' we first generate a set of L equidistant numbers $\{n_l : n_l = \aleph_{\min} + (l-1)\Delta n, l = 1, \ldots, L\}$, where $\Delta n = (\aleph_{\max} - \aleph_{\min})/(L-1)$. For each l, $l = 1, \ldots, L$, we assume that $n_l = n_e$ and compute the threshold using (33). This threshold is next substituted in (20) and (21) to compute the corresponding probability $P(\mathcal{H}_0^{p,r}|\mathcal{H}_1^{p,r})$. As the result a set of probabilities for the range of admissible thresholds is obtained, and η_2' is selected as the threshold for which the corresponding probability is closest to the required α_2.

REFERENCES

[1] D. Carevic, "Automatic estimation of multiple target positions and velocities using passive TDOA measurements of transients," *IEEE Trans. Signal Process.*, vol. 55, no. 2, pp. 424–436, Feb. 2007.

[2] N. Ueda and R. Nakano, "Deterministic annealing EM algorithm," *Neural Netw.*, vol. 11, no. 2, pp. 271–282, 1998.

[3] S. M. Kay, *Fundamentals of Statistical Signal Processing—Detection Theory*. Upper Saddle River, NJ: Prentice-Hall PTR, 1998.

[4] J. L. Spiesberger, "Identifying cross-correlation peaks due to multipaths with the application to optimal passive localization of transient signals and tomographic mapping of the environment," *J. Acoust. Soc. Amer.*, vol. 100, pp. 910–917, 1996.

[5] D. Carevic, "Robust estimation techniques for target-motion analysis using passively sensed transient signals," *IEEE J. Ocean. Eng.*, vol. 28, no. 2, pp. 250–261, 2003.

[6] D. Carevic, "Tracking target in cluttered environment using multilateral time-delay measurements," *J. Acoust. Soc. Amer.*, vol. 115, no. 3, pp. 1198–1206, 2004.

[7] B. G. Ferguson and J. L. Cleary, "In situ source level and source position estimates of biological transient signals produced by snapping shrimp in an underwater environment," *J. Acoust. Soc. Amer.*, vol. 109, no. 6, pp. 3031–3037, 2001.

[8] Y. Bar-Shalom and T. E. Fortman, *Tracking and Data Association*. New York: Academic, 1988.

[9] M. Abramowitz and I. A. Stegun, *Handbook of Mathematical Functions With Formulas, Graphs, and Mathematical Tables*. New York: Dover, 1964.

[10] D. B. Reid, "An algorithm for tracking multiple targets," *IEEE Trans. Autom. Control*, vol. 24, no. 6, pp. 843–854, 1979.

[11] R. P. S. Mahler, "Multitarget Bayes filtering via first-order multitarget moments," *IEEE Trans. Aerosp. Electron. Syst.*, vol. 39, no. 4, pp. 1152–1178, 2003.

[12] B. Vo, S. Singh, and A. Doucet, "Sequential Monte Carlo methods for multi-target filtering with finite random sets," *IEEE Trans. Aerosp. Electron. Syst.*, vol. 41, no. 4, pp. 1224–1245, 2005.

[13] R. Mahler, *Statistical Multisource-Multitarget Information Fusion*. Norwood, MA: Artech House, 2007.

[14] W. K. Ma, B. Vo, S. Singh, and A. Baddley, "Tracking an unknown time-varying number of speakers using TDOA measurements: A random finite set approach," *IEEE Trans. Signal Process.*, vol. 54, no. 9, pp. 3291–3304, Sep. 2006.

Four-Group Decodable Space–Time Block Codes

Dũng Ngọc Đào, *Member, IEEE*, Chau Yuen, *Member, IEEE*, Chintha Tellambura, *Senior Member, IEEE*, Yong Liang Guan, *Member, IEEE*, and Tjeng Thiang Tjhung, *Senior Member, IEEE*

***Abstract*—Two new rate-one full-diversity space–time block codes (STBCs) are proposed. They are characterized by the *lowest decoding complexity* among the known rate-one STBC, arising due to the complete separability of the transmitted symbols into four groups for maximum likelihood detection. The first and the second codes are delay-optimal if the number of transmit antennas is a power of 2 and even, respectively. The exact pairwise error probability is derived to allow for the performance optimization of the two codes. Compared with existing low-decoding complexity STBC, the two new codes offer several advantages such as higher code rate, lower encoding/decoding delay and complexity, lower peak-to-average power ratio, and better performance.**

***Index Terms*—Orthogonal designs, performance analysis, quasi-orthogonal space–time block codes, space–time block codes (STBC).**

I. INTRODUCTION

Space–time block codes (STBC[1]) have been extensively studied since they exploit the diversity and/or the capacity of multiple-input multiple-output (MIMO) channels. Among various STBC, orthogonal STBC (OSTBC) [1]–[3] offer the minimum decoding complexity and full diversity. However, they have low code rates when the number of transmit (Tx) antennas is more than 2 [3]. The rate of one symbol per channel use (pcu) only exists for two Tx antennas and the rate approaches 1/2 for a large number of Tx antennas [1]–[3].

To improve the low rate of OSTBC, several quasi-orthogonal STBC (QSTBC) have been proposed (see [4]–[7] and references therein). They allow joint maximum-likelihood (ML) decoding of pairs of complex symbols. However, the rate-one QSTBC exist for four Tx antennas only, and the code rate is smaller than 1 for more than four Tx antennas. Several rate-one STBC have been proposed (e.g., [8]–[10]), in which the transmitted symbols can be completely separated into two groups for ML detection. However, for more than four Tx antennas, the decoding complexity of the rate-one STBC in [8]–[10] increases significantly compared with OSTBC and QSTBC.

Manuscript received November 7, 2006; revised May 11, 2007. The associate editor coordinating the review of this manuscript and approving it for publication was Dr. Franz Hlawatsch. The work of D. N. Đào and C. Tellambura was supported by The National Sciences and Engineering Research Council (NSERC) and the Alberta Informatics Circle of Research Excellence (iCORE), Canada.

D. N. Đào was with Department of Electrical and Computer Engineering, University of Alberta, Edmonton, AB T6G 2V4, Canada. He is now with Department of Electrical and Computer Engineering, McGill University, Montréal, QC H3A 2A7, Canada (e-mail: ngoc.dao@mcgill.ca).

C. Yuen and T. T. Tjhung are with Institute for Infocomm Research, Singapore 119613 (e-mail: cyuen@i2r.a-star.edu.sg; tjhungtt@i2r.a-star.edu.sg).

C. Tellambura is with Department of Electrical and Computer Engineering, University of Alberta, Edmonton, AB T6G 2V4, Canada (e-mail: chintha@ece.ualberta.ca).

Y. L. Guan is with the School of Electrical and Electronic Engineering, Nanyang Technological University, Singapore, 639798 (e-mail: eylguan@ntu.edu.sg).

Digital Object Identifier 10.1109/TSP.2007.906729

[1]The term "STBC" stands for space–time block code/codes/coding, depending on the context.

TABLE I
COMPARISON OF SEVERAL LOW COMPLEXITY STBC FOR SIX AND EIGHT ANTENNAS. THE NUMBERS IN THE PARENTHESES INDICATE THE CODES' PARAMETERS FOR EIGHT Tx ANTENNAS

Codes	Maximal rate	Delay	Real symbol decoding
OSTBC [3], [24]	2/3 (5/8)	30 (56)	1 or 2 (1 or 2)
CIOD [17]	6/7 (4/5)	14 (50)	2 (2)
MDC-QSTBC [12]	3/4 (3/4)	8 (8)	2 (2)
QSTBC [6]	3/4 (3/4)	8 (8)	4 (4)
2Gp-QSTBC [8]	1 (1)	8 (8)	8 (8)
SAST [10]	1 (1)	6 (8)	6 (8)
4Gp-QSTBC (new)	**1** (**1**)	**8** (**8**)	**4** (**4**)
4Gp-SAST (new)	**1** (**1**)	**6** (**8**)	**3** (**4**)

In this paper, we propose two new rate-one STBC for any number of Tx antennas. Compared with the existing rate-one STBC, our new codes have lowest decoding complexity since the transmitted symbols can be decoupled into four groups (4Gp) for ML detection. The first code is called 4Gp-QSTBC. The second code is derived from semiorthogonal algebraic space–time (SAST) codes [10] and thus called 4Gp-SAST codes. The first and the second codes are delay-optimal when the number of Tx antennas is a power of 2 and even, respectively. The equivalent transmit–receive signals are derived so that sphere decoders [11] can be applied for data detection. To achieve full diversity, signal rotations are required for the two codes. The exact pairwise error probability (PEP) of the two codes is derived to optimize the signal rotations.

We compare the main parameters of our new codes, and several existing STBC for six and eight Tx antennas in Table I. Clearly, the new codes offer several distinct advantages such as higher code rate, low decoding complexity, and lower encoding/decoding delay. The two new codes also have lower peak-to-average power ratio (PAPR) than OSTBC, QSTBC, and minimum decoding complexity (MDC) QSTBC [12]. Moreover, simulation results show that our new codes also yield significant SNR gains compared with the existing codes.

Notation: Superscripts $^{\mathsf{T}}$, *, and † denote matrix transpose, conjugate, and transpose conjugate, respectively. The identity and all-zero square matrices of proper size are denoted by $\boldsymbol{I}$ and $\mathbf{0}$. The diagonal matrix with elements of vector $\boldsymbol{x}$ on the main diagonal is denoted by $\mathrm{diag}(\boldsymbol{x})$. $\|X\|_{\mathsf{F}}$ stands for the Frobenius norm of matrix X and $\otimes$ denotes Kronecker product [13]. A mean-m and variance-σ^2 circularly complex Gaussian random variable is written by $\mathcal{CN}(m,\sigma^2)$. $\Re(X)$ and $\Im(X)$ denote the real and imaginary parts of X, respectively.

II. SYSTEM MODEL AND PRELIMINARIES

A. System Model

We consider data transmission over a MIMO quasi-static Rayleigh flat-fading channel with M Tx and N receive (Rx) antennas [14]. The channel gain h_{mn} $(m = 1,2,\ldots,M;\ n = 1,2,\ldots,N)$ between the (m,n)th Tx–Rx antenna pair is assumed $\mathcal{CN}(0,1)$ and remains constant over T time slots. We assume no spatial correlation at either Tx or Rx array. The receiver, but not the transmitter, completely knows the channel gains.

A $T \times M$ STBC can be represented in a general dispersion form [14] as follows:

$$X = \sum_{k=1}^{K} (a_k A_k + b_k B_k) \tag{1}$$

where A_k and B_k, $(k = 1,2,\cdots,K)$ are $T \times M$ constant matrices, commonly called dispersion matrices; a_k and b_k are the real and imaginary parts of the symbol s_k. We can use an equivalent form of STBC as

$$X = \sum_{l=1}^{L} c_l C_l \tag{2}$$

where L is the number (not necessarily even) of transmitted symbols, c_l are real-value transmitted symbols, C_l are dispersion matrices. The average energy of code matrices is constrained such that $\mathcal{E}_{\mathcal{X}} = \mathbb{E}[\|X\|_{\mathsf{F}}^2] = T$.

The received signals y_{tn} of the nth antenna at time t can be arranged in a matrix Y of size $T \times N$. Thus, one can represent the Tx–Rx signal relation as [14], [15]

$$Y = \sqrt{\rho} X H + Z \tag{3}$$

where $H = [h_{mn}]$ is the channel matrix; $Z = [z_{tn}]$ is the noise matrix of size $T \times N$, its elements z_{tn} are independently, identically distributed (i.i.d.) $\mathcal{CN}(0,1)$. The Tx power is scaled by ρ so that the average signal-to-noise ratio (SNR) at each Rx antenna is ρ, independent of the number of Tx antennas.

Let the data vector be $\boldsymbol{c} = [c_1\ c_2\ \ldots c_L]^{\mathsf{T}}$. The ML decoding of STBC is to find the solution $\hat{\boldsymbol{c}}$ so that

$$\hat{\boldsymbol{c}} = \arg\min_{\boldsymbol{c}} \|Y - XH\|_{\mathsf{F}}^2. \tag{4}$$

B. Algebraic Constraints of QSTBC

The key idea of QSTBC is to divide the L (real) transmitted symbols embedded in a code matrix into Γ groups, so that the ML detection of the transmitted symbol vector can be decoupled into Γ submetrics; each metric involves the symbols of only one group [6], [8], [10], [16]. We provide a definition of STBC with this feature to unify the notation in this paper as follows.

Definition 1: An STBC is said to be Γ-group decodable STBC if the ML decoding metric (4) can be decoupled into a linear sum of Γ independent submetrics, each submetric consists of the symbols from only one group. The Γ-group decodable STBC is denoted by Γ Gp-STBC for short.

In the most general case, we assume that there are Γ groups; each group is denoted by Ω_i $(i = 1,2,\ldots,\Gamma)$ and has L_i symbols. Thus, $L = \sum_{i=1}^{\Gamma} L_i$. Let Θ_i be the set of indexes of symbols in the group Ω_i.

Yuen *et al.* [16, Theorem 1] have shown a sufficient condition for an STBC to be Γ-group decodable. In fact, this condition is also necessary. We will state these results in the following theorem without proof for brevity.

Theorem 1: The necessary and sufficient conditions, so that an STBC is Γ-group decodable, are

$$C_p^{\dagger} C_q + C_q^{\dagger} C_p = \mathbf{0} \quad \forall p \in \Theta_i \quad \forall q \in \Theta_j, i \neq j. \tag{5}$$

Note that Theorem 1 covers [17, Theorem 9] (single-symbol decodable STBC) and can be shown similarly.

III. FOUR-GROUP DECODABLE STBC DERIVED FROM QSTBC

A. Encoding

In this section, we will study the new 4Gp-QSTBC. As we will see later, the general form of STBC in (1) is convenient for studying 4Gp-QSTBC; hence Theorem 1 can be restated as follows.

Lemma 1 ([18]): The necessary and sufficient conditions for an STBC in (1) to become Γ-group decodable are a) $A_p^\dagger A_q + A_p^\dagger A_q = \mathbf{0}$, b) $B_p^\dagger B_q + B_p^\dagger B_q = \mathbf{0}$, and c) $A_p^\dagger B_q + B_p^\dagger A_q = \mathbf{0}, \forall p \in \Theta_i, \forall q \in \Theta_j$, $1 \le i \ne j \le \Gamma$.

We next consider another sufficient condition so that an STBC is four-group decodable.

Theorem 2: Given a 4Gp-STBC for M Tx antennas with code length T and K sets of dispersion matrices $(A_k, B_k; 1 \le k \le K)$, a 4Gp-STBC with code length $2T$ for $2M$ Tx antennas, which consists of $2K$ sets of dispersion matrices denoted as $(\bar{A}_i, \bar{B}_i)$, $1 \le i \le 2K$, can be constructed using the following mapping rules:

$$\bar{A}_{2k-1} = \begin{bmatrix} A_k & \mathbf{0} \\ \mathbf{0} & A_k \end{bmatrix}, \quad \bar{A}_{2k} = \begin{bmatrix} B_k & \mathbf{0} \\ \mathbf{0} & B_k \end{bmatrix}$$
$$\bar{B}_{2k-1} = \begin{bmatrix} \mathbf{0} & A_k \\ A_k & \mathbf{0} \end{bmatrix}, \ \bar{B}_{2k} = \begin{bmatrix} \mathbf{0} & B_k \\ B_k & \mathbf{0} \end{bmatrix}. \tag{6}$$

Proof: Theorem 2 can be proved by showing that if the dispersion matrices $(A_q, B_q)(1 \le q \le K)$ satisfy Lemma 1 with $(A_p, B_p)(1 \le p \le K)$, where $q \notin \Theta_p$, then the dispersion matrices $(\bar{A}_{2q-1}, \bar{B}_{2q-1}, \bar{A}_{2q}, \bar{B}_{2q})$ constructed from (A_q, B_q) using (6) will satisfy Theorem 2 with $(\bar{A}_{2p-1}, \bar{B}_{2p-1}, \bar{A}_{2p}, \bar{B}_{2p})$ constructed from (A_p, B_p) using (6). The detailed proof is omitted here, as the steps are routine. □

The recursive construction of 4Gp-STBC specified in Theorem 2 suggests that we can start with the MDC-QSTBC for four Tx antennas proposed in [12] to construct 4Gp-STBC for eight, 16 Tx antennas, and so on, because MDC-QSTBC is one of the STBC satisfying Lemma 1; the resulting STBC is thus called 4Gp-QSTBC. For practical interest, we will illustrate the encoding process of 4Gp-QSTBC for eight Tx antennas from the MDC-QSTBC for four Tx antennas [12]. The code matrix of MDC-QSTBC for four Tx antennas is

$$F_4 = \begin{bmatrix} a_1 + \mathrm{j}a_3 & a_2 + \mathrm{j}a_4 & b_1 + \mathrm{j}b_3 & b_2 + \mathrm{j}b_4 \\ -a_2 + \mathrm{j}a_4 & a_1 - \mathrm{j}a_3 & -b_2 + \mathrm{j}b_4 & b_1 - \mathrm{j}b_3 \\ b_1 + \mathrm{j}b_3 & b_2 + \mathrm{j}b_4 & a_1 + \mathrm{j}a_3 & a_2 + \mathrm{j}a_4 \\ -b_2 + \mathrm{j}b_4 & b_1 - \mathrm{j}b_3 & -a_2 + \mathrm{j}a_4 & a_1 - \mathrm{j}a_3 \end{bmatrix} \tag{7}$$

where $\mathrm{j}^2 = -1$.

The code matrix of 4Gp-QSTBC for eight Tx antennas from F_4 using mapping rules in (6) is given in (8), shown at the bottom of the page.

The code rate of 4Gp-QSTBC for eight Tx antennas is one symbol pcu. In general, by construction, the rate of 4Gp-QSTBC for $2M$ Tx antennas is the same as the rate of MDC-QSTBC for M Tx antennas. The maximal rate of MDC-QSTBC is one symbol pcu [12], the maximal achievable rate of 4Gp-QSTBC is also one symbol pcu for 2^m Tx antennas. If the number of Tx antennas is $M < 2^m$ $(m = 2, 3, \ldots)$, then $(2^m - M)$ columns of the code matrix for 2^m Tx antennas can be deleted to obtain the code for M antennas. Thus, *the maximum rate of 4Gp-QSTBC is one symbol pcu, and it is achievable for any number of Tx antennas*. In addition, the 4×4 code matrix F_4 is square. By recursive construction (6), the code matrices of 4Gp-QSTBC are also square for 2^m Tx antennas; and therefore, 4Gp-QSTBCs are delay optimal if the number of Tx antennas is 2^m [17].

B. Decoding

We know that the symbols s_1, s_2, s_3, s_4 of F_4 can be separately detected [12]. Therefore, from Theorem 2, the four groups of eight symbols of F_8 can be detected independently. These four groups are (s_1, s_2), (s_3, s_4), (s_5, s_6), and (s_7, s_8). The ML metric given in (4) can be derived to detect the four groups of symbols of F_8. However, to provide more insights into the decoding of 4Gp-QSTBC, we will derive an equivalent code and the equivalent channel of F_8. Furthermore, using the equivalent channel of F_8, we can use a sphere decoder [11] to reduce the complexity of the ML search.

The equivalent code of F_8 is obtained by column permutations for the code matrix of F_8 in (8): the order of columns is changed to (1, 3, 5, 7, 2, 4, 6, 8). This order of permutations is also applied for the rows of F_8. Letting $x_1 = a_1 + \mathrm{j}a_5$, $x_2 = a_2 + \mathrm{j}a_6$, $x_3 = b_1 + \mathrm{j}b_5$, $x_4 = b_2 + \mathrm{j}b_6$, $x_5 = a_3 + \mathrm{j}a_7$, $x_6 = a_4 + \mathrm{j}a_8$, $x_7 = b_3 + \mathrm{j}b_7$, and $x_8 = b_4 + \mathrm{j}b_8$ be the intermediate variables, we obtain a permutation-equivalent code of F_8, as follows:

$$D = \begin{bmatrix} \mathcal{D}_1 & \mathcal{D}_2 \\ -\mathcal{D}_2^* & \mathcal{D}_1^* \end{bmatrix} \tag{9}$$

where

$$\mathcal{D}_1 = \begin{bmatrix} x_1 & x_2 & x_3 & x_4 \\ x_2 & x_1 & x_4 & x_3 \\ x_3 & x_4 & x_1 & x_2 \\ x_4 & x_3 & x_2 & x_1 \end{bmatrix}, \quad \mathcal{D}_2 = \begin{bmatrix} x_5 & x_6 & x_7 & x_8 \\ x_6 & x_5 & x_8 & x_7 \\ x_7 & x_8 & x_5 & x_6 \\ x_8 & x_7 & x_6 & x_5 \end{bmatrix}. \tag{10}$$

The submatrices $\mathcal{D}_1$ and $\mathcal{D}_2$ have a special form called *block-circulant matrix with circulant blocks* [13].

We next show how to decode the code D. For simplicity, a single Rx antenna is considered. The generalization for multiple Rx antennas is straightforward. Assume that the Tx symbols are drawn from a constellation with unit average power; the Tx–Rx signal model in (3) for the case of STBC D follows:

$$\boldsymbol{y} = \sqrt{\rho/8} D \boldsymbol{h} + \boldsymbol{z}. \tag{11}$$

$$F_8 = \begin{bmatrix} a_1 + \mathrm{j}a_5 & a_3 + \mathrm{j}a_7 & a_2 + \mathrm{j}a_6 & a_4 + \mathrm{j}a_8 & b_1 + \mathrm{j}b_5 & b_3 + \mathrm{j}b_7 & b_2 + \mathrm{j}b_6 & b_4 + \mathrm{j}b_8 \\ -a_3 + \mathrm{j}a_7 & a_1 - \mathrm{j}a_5 & -a_4 + \mathrm{j}a_8 & a_2 - \mathrm{j}a_6 & -b_3 + \mathrm{j}b_7 & b_1 - \mathrm{j}b_5 & -b_4 + \mathrm{j}b_8 & b_2 - \mathrm{j}b_6 \\ a_2 + \mathrm{j}a_6 & a_4 + \mathrm{j}a_8 & a_1 + \mathrm{j}a_5 & a_3 + \mathrm{j}a_7 & b_2 + \mathrm{j}b_6 & b_4 + \mathrm{j}b_8 & b_1 + \mathrm{j}b_5 & b_3 + \mathrm{j}b_7 \\ -a_4 + \mathrm{j}a_8 & a_2 - \mathrm{j}a_6 & -a_3 + \mathrm{j}a_7 & a_1 - \mathrm{j}a_5 & -b_4 + \mathrm{j}b_8 & b_2 - \mathrm{j}b_6 & -b_3 + \mathrm{j}b_7 & b_1 - \mathrm{j}b_5 \\ b_1 + \mathrm{j}b_5 & b_3 + \mathrm{j}b_7 & b_2 + \mathrm{j}b_6 & b_4 + \mathrm{j}b_8 & a_1 + \mathrm{j}a_5 & a_3 + \mathrm{j}a_7 & a_2 + \mathrm{j}a_6 & a_4 + \mathrm{j}a_8 \\ -b_3 + \mathrm{j}b_7 & b_1 - \mathrm{j}b_5 & -b_4 + \mathrm{j}b_8 & b_2 - \mathrm{j}b_6 & -a_3 + \mathrm{j}a_7 & a_1 - \mathrm{j}a_5 & -a_4 + \mathrm{j}a_8 & a_2 - \mathrm{j}a_6 \\ b_2 + \mathrm{j}b_6 & b_4 + \mathrm{j}b_8 & b_1 + \mathrm{j}b_5 & b_3 + \mathrm{j}b_7 & a_2 + \mathrm{j}a_6 & a_4 + \mathrm{j}a_8 & a_1 + \mathrm{j}a_5 & a_3 + \mathrm{j}a_7 \\ -b_4 + \mathrm{j}b_8 & b_2 - \mathrm{j}b_6 & -b_3 + \mathrm{j}b_7 & b_1 - \mathrm{j}b_5 & -a_4 + \mathrm{j}a_8 & a_2 - \mathrm{j}a_6 & -a_3 + \mathrm{j}a_7 & a_1 - \mathrm{j}a_5 \end{bmatrix}. \tag{8}$$

Let $\boldsymbol{x} = [x_1\ x_2\ \ldots\ x_8]^{\mathsf{T}}$, $\hat{\boldsymbol{y}} = [y_1\ \ldots\ y_4\ y_5^*\ \ldots\ y_8^*]^{\mathsf{T}}$, $\hat{\boldsymbol{z}} = [z_1\ \ldots\ z_4\ z_5^*\ \ldots\ z_8^*]^{\mathsf{T}}$, and

$$\mathcal{H}_1 = \begin{bmatrix} h_1 & h_2 & h_3 & h_4 \\ h_2 & h_1 & h_4 & h_3 \\ h_3 & h_4 & h_1 & h_2 \\ h_4 & h_3 & h_2 & h_1 \end{bmatrix}, \quad \mathcal{H}_2 = \begin{bmatrix} h_5 & h_6 & h_7 & h_8 \\ h_6 & h_5 & h_8 & h_7 \\ h_7 & h_8 & h_5 & h_6 \\ h_8 & h_7 & h_6 & h_5 \end{bmatrix}. \quad (12)$$

We have an equivalent expression of (11) as

$$\hat{\boldsymbol{y}} = \sqrt{\frac{\rho}{8}} \underbrace{\begin{bmatrix} \mathcal{H}_1 & \mathcal{H}_2 \\ \mathcal{H}_2^* & -\mathcal{H}_1^* \end{bmatrix}}_{\bar{\mathcal{H}}} \boldsymbol{x} + \hat{\boldsymbol{z}}. \quad (13)$$

Note that $\mathcal{H}_1$ and $\mathcal{H}_2$ are block-circulant matrices with circulant-blocks [13]. Thus, they are commutative and so do $\mathcal{H}_1^*$ and $\mathcal{H}_2^*$. We can multiply both sides of (13) with $\bar{\mathcal{H}}^{\dagger}$ to get

$$\underbrace{\bar{\mathcal{H}}^{\dagger}\hat{\boldsymbol{y}}}_{\bar{\boldsymbol{y}}} = \sqrt{\frac{\rho}{8}} \begin{bmatrix} \mathcal{H}_1^*\mathcal{H}_1 + \mathcal{H}_2^*\mathcal{H}_2 & \mathbf{0} \\ \mathbf{0} & \mathcal{H}_1^*\mathcal{H}_1 + \mathcal{H}_2^*\mathcal{H}_2 \end{bmatrix} \boldsymbol{x} + \underbrace{\bar{\mathcal{H}}^{\dagger}\hat{\boldsymbol{z}}}_{\bar{\boldsymbol{z}}}. \quad (14)$$

It can be shown that the noise elements of vector $\bar{\boldsymbol{z}}$ are correlated with covariance matrix $\bar{\mathcal{H}}^{\dagger}\bar{\mathcal{H}}$. Thus, this noise vector can be whitened by multiplying both side of (14) with the matrix $(\bar{\mathcal{H}}^{\dagger}\bar{\mathcal{H}})^{-1/2}$. Let $\hat{\mathcal{H}} = \mathcal{H}_1^*\mathcal{H}_1 + \mathcal{H}_2^*\mathcal{H}_2$. After the noise whitening step, (14) is equivalent to the following equations:

$$\hat{\mathcal{H}}^{-1/2}\bar{\boldsymbol{y}}_i = \sqrt{\frac{\rho}{8}}\hat{\mathcal{H}}^{1/2}\boldsymbol{x}_i + \bar{\boldsymbol{z}}_i, \qquad (i = 1, 2) \quad (15)$$

where $\bar{\boldsymbol{y}}_i = [\bar{y}_{4i-3}\ \bar{y}_{4i-2}\ \bar{y}_{4i-1}\ \bar{y}_{4i}]^{\mathsf{T}}$, $\boldsymbol{x}_i = [x_{4i-3}\ x_{4i-2}\ x_{4i-1}\ x_{4i}]^{\mathsf{T}}$, the noise vectors $\bar{\boldsymbol{z}}_i = [\hat{\mathcal{H}}^{-1/2}\bar{z}_{4i-3}\ \bar{z}_{4i-2}\ \bar{z}_{4i-1}\ \bar{z}_{4i}]^{\mathsf{T}}$ are uncorrelated and have elements $\sim \mathcal{CN}(0, 1)$.

At this point, the decoding of the eight transmitted symbols of the code D can be readily decoupled into two groups. However, since the code is a 4Gp-STBC, we can further decompose them into four groups in the following.

Denote the 2×2 (real) discrete Fourier transform (DFT) matrix by

$$\mathcal{F}_2 = \begin{bmatrix} 1 & 1 \\ 1 & -1 \end{bmatrix}.$$

The block-circulant matrices $\mathcal{H}_1$ and $\mathcal{H}_2$ can be diagonalized by a (real) unitary matrix $\Theta = (1/2)\mathcal{F}_2 \otimes \mathcal{F}_2$ [13, Theorem 5.8.2, p. 185]. Note that $\Theta^{\dagger} = \Theta$, therefore, $\mathcal{H}_1 = \Theta\Lambda_1\Theta$ and $\mathcal{H}_2 = \Theta\Lambda_2\Theta$, where Λ_1 and Λ_2 are diagonal matrices, with eigenvalues of $\mathcal{H}_1$ and $\mathcal{H}_2$ in the main diagonal, respectively. Thus, $\hat{\mathcal{H}} = \Theta(\Lambda_1^{\dagger}\Lambda_1 + \Lambda_2^{\dagger}\Lambda_2)\Theta$, and also $\hat{\mathcal{H}}^{1/2} = \Theta(\Lambda_1^{\dagger}\Lambda_1 + \Lambda_2^{\dagger}\Lambda_2)^{1/2}\Theta$. Since $\hat{\mathcal{H}}^{1/2}$ is a real matrix, (15) becomes

$$\hat{\mathcal{H}}^{-1/2}\Re(\bar{\boldsymbol{y}}_i) = \sqrt{\rho/8}\hat{\mathcal{H}}^{1/2}\Re(\boldsymbol{x}_i) + \Re(\bar{\boldsymbol{z}}_i), \quad i = 1, 2, \quad (16a)$$

$$\hat{\mathcal{H}}^{-1/2}\Im(\bar{\boldsymbol{y}}_i) = \sqrt{\rho/8}\hat{\mathcal{H}}^{1/2}\Im(\boldsymbol{x}_i) + \Im(\bar{\boldsymbol{z}}_i), \quad i = 1, 2. \quad (16b)$$

Note that $\Re(\boldsymbol{x}_1) = [a_1\ a_2\ b_1\ b_2]^{\mathsf{T}} := \boldsymbol{d}_1$, i.e., $\Re(\boldsymbol{x}_1)$ is only dependent on the complex symbols s_1 and s_2. Similarly, $\Re(\boldsymbol{x}_2)$, $\Im(\boldsymbol{x}_1)$, and $\Im(\boldsymbol{x}_2)$ depend on (s_3, s_4), (s_5, s_6), and (s_7, s_8), respectively.

Equation (16) shows that the decoding of eight transmitted symbols of STBC D is separated into the decoding of four groups, each with two symbols (thus the search space size has been reduced from Q^8 to $4Q^2$ where Q is the transmit constellation size). A sphere decoder [11] can also be used to reduce the complexity of the ML search for each group. The matrix $\hat{\mathcal{H}}^{1/2}$ can be considered as the *equivalent channel* of the 4Gp-QSTBC D.

C. Performance Analysis

In (16), the PEP of the four transmit symbol vectors are the same. We thus need to consider the PEP of one of the vectors $\boldsymbol{d}_1 = \Re(\boldsymbol{x}_1) = [a_1\ a_2\ b_1\ b_2]^{\mathsf{T}}$. For notational simplicity, the subindex 1 of $\boldsymbol{d}_1$ is dropped. In addition, we can introduce redundancy on the signal space by using a 4×4 real unitary rotation R to the data vector $[a_1\ a_2\ b_1\ b_2]^{\mathsf{T}}$. Thus, the data vector $\boldsymbol{d} = R[a_1\ a_2\ b_1\ b_2]^{\mathsf{T}}$.

From (16a), the PEP of the pair $\boldsymbol{d}$ and $\bar{\boldsymbol{d}}$ can be expressed by the Gaussian tail function as [19]

$$\begin{aligned} P(\boldsymbol{d} \to \bar{\boldsymbol{d}}|\hat{\mathcal{H}}) &= Q\left(\sqrt{\frac{\rho}{8}\frac{\|\hat{\mathcal{H}}^{1/2}R\boldsymbol{\delta}\|_{\mathsf{F}}^2}{4N_0}}\right) \\ &= Q\left(\sqrt{\frac{\rho\left[\boldsymbol{\delta}^{\mathsf{T}}R^{\mathsf{T}}\Theta^{\mathsf{T}}\left(\Lambda_1^{\dagger}\Lambda_1 + \Lambda_2^{\dagger}\Lambda_2\right)\Theta R\boldsymbol{\delta}\right]}{16}}\right). \end{aligned} \quad (17)$$

where $\boldsymbol{\delta} = \boldsymbol{d} - \bar{\boldsymbol{d}}$, $N_0 = 1/2$ is the variance of the elements of the white noise vector $\Re(\boldsymbol{z}_1)$ in (16a).

Remember that Λ_1 is a diagonal matrix with eigenvalues of $\mathcal{H}_1$ on the main diagonal. Let $\lambda_{i,j}$ $(i = 1, 2; j = 1, 2, 3, 4)$ be the eigenvalues of $\mathcal{H}_i$. Then $\Lambda_i = \mathrm{diag}(\lambda_{i,1}, \lambda_{i,2}, \lambda_{i,3}, \lambda_{i,4})$. Let $\boldsymbol{\beta} = \Theta R\boldsymbol{\delta}$, we have

$$P(\boldsymbol{d} \to \bar{\boldsymbol{d}}|\hat{\mathcal{H}}) = Q\left(\sqrt{\frac{\rho\left(\sum_{i=1}^{2}\sum_{j=1}^{4}\beta_j^2|\lambda_{i,j}|^2\right)}{16}}\right). \quad (18)$$

To derive a closed form of (18), we need to evaluate the distribution of $\lambda_{i,j}$. The eigenvectors of $\mathcal{H}_1$ is the columns of the matrix $\Theta = (1/2)\mathcal{F}_2 \otimes \mathcal{F}_2$. Thus, the eigenvalues of $\mathcal{H}_1$ are $[\lambda_{1,1}\ \lambda_{1,2}\ \lambda_{1,3}\ \lambda_{1,4}]^{\mathsf{T}} = (\mathcal{F}_2 \otimes \mathcal{F}_2)[h_1\ h_2\ h_3\ h_4]^{\mathsf{T}}$. Since $h_j \sim \mathcal{CN}(0, 1)$ for $(j = 1, \ldots, 4)$, thus $\lambda_{1,j} \sim \mathcal{CN}(0, 4)$ and so do $\lambda_{2,j}$.

We now use the Craig's formula [20] to derive the conditional PEP in (18), as follows:

$$\begin{aligned} P(\boldsymbol{d} \to \bar{\boldsymbol{d}}|\hat{\mathcal{H}}) &= Q\left(\sqrt{\frac{\rho\left(\sum_{i=1}^{2}\sum_{j=1}^{4}\beta_j^2|\lambda_{i,j}|^2\right)}{16}}\right) \\ &= \frac{1}{\pi}\int_0^{\pi/2}\exp\left(\frac{-\rho\left(\sum_{i=1}^{2}\sum_{j=1}^{4}\beta_j^2|\lambda_{i,j}|^2\right)}{32\sin^2\alpha}\right)d\alpha. \end{aligned} \quad (19)$$

Applying a method based on the moment-generating function [19], we obtain the unconditional PEP as

$$P(\boldsymbol{d} \to \bar{\boldsymbol{d}}) = \frac{1}{\pi}\int_0^{\pi/2}\left[\prod_{i=1}^{4}\left(1 + \frac{\rho\beta_i^2}{8\sin^2\alpha}\right)\right]^{-2}d\alpha. \quad (20)$$

If $\beta_i \neq 0\ \forall i = 1,\ldots,4$, then $1 + (\rho\beta_i^2/8\sin^2\alpha) \approx (\rho\beta_i^2/8\sin^2\alpha)$ at high SNR, the approximation of the exact PEP in (20) is

$$P(\boldsymbol{d}\to\bar{\boldsymbol{d}}) \approx \left(\frac{2^{24}\rho^{-8}}{\pi}\int_0^{\pi/2}(\sin\alpha)^{16}d\alpha\right)\prod_{i=1}^{4}|\beta_i|^{-4} = \frac{2^7 16!\rho^{-8}}{8!8!}\prod_{i=1}^{4}|\beta_i|^{-4}. \quad (21)$$

The exponent of SNR in (21) is -8. This indicates that the maximum diversity order of 4Gp-QSTBC is 8, and it is achievable if the product distance $\prod_{i=1}^{4}\beta_i$ (see [21] and references therein) is nonzero for all possible data vectors. Furthermore, at high SNR, the asymptotic PEP becomes very tight to the exact PEP. Recall that $\boldsymbol{\beta} = \Theta R(\boldsymbol{d}-\bar{\boldsymbol{d}})$; thus, the product matrix ΘR is the combined rotation matrix for data vector $\boldsymbol{d}$. Since Θ is a constant matrix, we can optimize the matrix R so that the minimum product distance $d_{p,\min} = \min_{\forall \boldsymbol{d}^i,\boldsymbol{d}^j}\prod_{k=1}^{4}|\beta_k|$, where $\boldsymbol{\beta} = [\Theta R(\boldsymbol{d}^i - \boldsymbol{d}^j)]$ is nonzero and maximized.

If the complex signals are drawn from QAM, the (real) elements of $\boldsymbol{d}$ are in the set $\{\pm1,\pm3,\pm5,\ldots\}$. The best known rotations for QAM in terms of maximizing the minimum product distance are provided in [21] and [22]. Denoting the rotation matrix in [21] and [22] by R_{BOV}, the signal rotation for our 4Gp-QSTBC is given by

$$R = \Theta R_{BOV}. \quad (22)$$

Simulations show that the above vector signal rotation perform better than the symbolwise rotation proposed in [18] (details omitted for brevity).

We have presented important properties of 4Gp-QSTBC. In the next section, we will investigate 4Gp-SAST codes.

IV. Four-Group Decodable STBC Derived From SAST Codes

A. Encoding

The SAST code matrix is constructed for $M = 2\bar{M}$ Tx antennas using circulant blocks. Two length-$\bar{M}$ data vectors $\boldsymbol{s}_1 = [s_1\ s_2\ \ldots\ s_{\bar{M}}]^{\mathsf{T}}$ and $\boldsymbol{s}_2 = [s_{\bar{M}+1}\ s_{\bar{M}+2}\ \ldots\ s_{2\bar{M}}]^{\mathsf{T}}$ are used to generate two $\bar{M}$-by-$\bar{M}$ circulant matrices [13]. Note that the first row of circulant matrix $\mathcal{C}(\boldsymbol{x})$ copies the row vector $\boldsymbol{x}$; the ith row is obtained by circular shift $(i-1)$ times to the right the vector $\boldsymbol{x}$. The SAST code matrix is constructed as

$$\mathcal{S} = \begin{bmatrix} \mathcal{C}\left(\boldsymbol{s}_1^{\mathsf{T}}\right) & \mathcal{C}\left(\boldsymbol{s}_2^{\mathsf{T}}\right) \\ -\mathcal{C}^{\dagger}\left(\boldsymbol{s}_2^{\mathsf{T}}\right) & \mathcal{C}^{\dagger}\left(\boldsymbol{s}_1^{\mathsf{T}}\right)\end{bmatrix}. \quad (23)$$

By construction, 4Gp-SAST codes have rate of one symbol pcu; the code matrices for an even number of Tx antennas are square; thus, 4Gp-SAST codes are delay-optimal for an even number of Tx antennas.

B. Decoder of 4Gp-SAST Codes

Similar to 4Gp-QSTBC, the decoding of 4Gp-SAST codes requires two steps. First, the two data vectors $\boldsymbol{s}_1$ and $\boldsymbol{s}_2$ are decoupled [10]; then, the real and imaginary parts of vectors $\boldsymbol{s}_1$ and $\boldsymbol{s}_2$ are separated. We provide the detail decoder with only one Rx antenna as generalization for multiple Rx antennas can be easily done.

We introduce another type of circulant matrix called left circulant, denoted by $\mathcal{C}_L(\boldsymbol{x})$, where the ith row is obtained by circular shifts $(i-1)$ times to the left for the row vector $\boldsymbol{x}$.

Let us define a permutation Π on an arbitrary $M\times M$ matrix X such that, the $(M-i+2)$th row is permuted with the ith row for $i = 2,3,\ldots,\lceil M/2\rceil$, where $\lceil(\cdot)\rceil$ is the ceiling function. One can verify that

$$\Pi\left(\mathcal{C}_L(\boldsymbol{x})\right) = \mathcal{C}(\boldsymbol{x}). \quad (24)$$

Let $\boldsymbol{y} = [\boldsymbol{y}_1^{\mathsf{T}}\ \boldsymbol{y}_2^{\mathsf{T}}]^{\mathsf{T}}$, $\boldsymbol{y}_1 = [y_1\ y_2\ \ldots\ y_{\bar{M}}]^{\mathsf{T}}$, $\boldsymbol{y}_2 = [y_{\bar{M}+1}\ y_{\bar{M}+2}\ \ldots\ y_M]^{\mathsf{T}}$, $\boldsymbol{h} = [\boldsymbol{h}_1^{\mathsf{T}}\ \boldsymbol{h}_2^{\mathsf{T}}]^{\mathsf{T}}$, $\boldsymbol{h}_1 = [h_1\ h_2\ \ldots\ h_{\bar{M}}]^{\mathsf{T}}$, $\boldsymbol{h}_2 = [h_{\bar{M}+1}\ h_{\bar{M}+2}\ \ldots\ h_{2\bar{M}}]^{\mathsf{T}}$, $\boldsymbol{z} = [\boldsymbol{z}_1^{\mathsf{T}}\ \boldsymbol{z}_2^{\mathsf{T}}]^{\mathsf{T}}$, $\boldsymbol{z}_1 = [z_1\ z_2\ \ldots\ z_{\bar{M}}]^{\mathsf{T}}$, $\boldsymbol{z}_2 = [z_{\bar{M}+1}\ z_{\bar{M}+2}\ \ldots\ z_{2\bar{M}}]^{\mathsf{T}}$. We can write the Tx–Rx signal relation as

$$\begin{bmatrix}\boldsymbol{y}_1\\ \boldsymbol{y}_2\end{bmatrix} = \sqrt{\frac{\rho}{M}}\begin{bmatrix}\mathcal{C}(\boldsymbol{s}_1) & \mathcal{C}(\boldsymbol{s}_2)\\ -\mathcal{C}^{\dagger}(\boldsymbol{s}_2) & \mathcal{C}^{\dagger}(\boldsymbol{s}_1)\end{bmatrix}\begin{bmatrix}\boldsymbol{h}_1\\ \boldsymbol{h}_2\end{bmatrix} + \begin{bmatrix}\boldsymbol{z}_1\\ \boldsymbol{z}_2\end{bmatrix}. \quad (25)$$

An equivalent form of (25) is

$$\begin{bmatrix}\boldsymbol{y}_1\\ \boldsymbol{y}_2^*\end{bmatrix} = \sqrt{\frac{\rho}{M}}\begin{bmatrix}X_1 & X_2\\ X_3 & X_4\end{bmatrix}\begin{bmatrix}\boldsymbol{s}_1\\ \boldsymbol{s}_2\end{bmatrix} + \begin{bmatrix}\boldsymbol{z}_1\\ \boldsymbol{z}_2^*\end{bmatrix} \quad (26)$$

where $X_1 = \mathcal{C}_L(\boldsymbol{h}_1^{\mathsf{T}})$, $X_2 = \mathcal{C}_L(\boldsymbol{h}_2^{\mathsf{T}})$, $X_3 = \mathcal{C}^{\dagger}(\boldsymbol{h}_2^{\mathsf{T}})$, $X_4 = -\mathcal{C}^{\dagger}(\boldsymbol{h}_1^{\mathsf{T}})$.

Applying permutation Π in (24) for the column matrix $\boldsymbol{y}_1$, we obtain

$$\begin{aligned}\begin{bmatrix}\bar{\boldsymbol{y}}_1\\ \bar{\boldsymbol{y}}_2\end{bmatrix} &\triangleq \begin{bmatrix}\Pi(\boldsymbol{y}_1)\\ \boldsymbol{y}_2^*\end{bmatrix}\\ &= \sqrt{\frac{\rho}{M}}\begin{bmatrix}\Pi(X_1) & \Pi(X_2)\\ X_3 & X_4\end{bmatrix}\begin{bmatrix}\boldsymbol{s}_1\\ \boldsymbol{s}_2\end{bmatrix} + \begin{bmatrix}\Pi(\boldsymbol{z}_1)\\ \boldsymbol{z}_2^*\end{bmatrix}\\ &= \sqrt{\frac{\rho}{M}}\underbrace{\begin{bmatrix}H_1 & H_2\\ H_2^{\dagger} & -H_1^{\dagger}\end{bmatrix}}_{\mathcal{H}}\begin{bmatrix}\boldsymbol{s}_1\\ \boldsymbol{s}_2\end{bmatrix} + \begin{bmatrix}\bar{\boldsymbol{z}}_1\\ \bar{\boldsymbol{z}}_2\end{bmatrix}\end{aligned} \quad (27)$$

where $H_1 = \mathcal{C}(\boldsymbol{h}_1^{\mathsf{T}})$, $H_2 = \mathcal{C}(\boldsymbol{h}_2^{\mathsf{T}})$, $\bar{\boldsymbol{z}}_1 = \Pi(\boldsymbol{z}_1)$, $\bar{\boldsymbol{z}}_2 = \boldsymbol{z}_2^*$. The elements of $\bar{\boldsymbol{z}}_1$ and $\bar{\boldsymbol{z}}_2$ are $\sim\mathcal{CN}(0,1)$, as elements of $\boldsymbol{z}_1$ and $\boldsymbol{z}_2$. We now multiply $\mathcal{H}^{\dagger}$ with both sides of (27). Letting $\hat{\mathcal{H}} = H_1^{\dagger}H_1 + H_2^{\dagger}H_2$, we get

$$\begin{aligned}\begin{bmatrix}\hat{\boldsymbol{y}}_1\\ \hat{\boldsymbol{y}}_2\end{bmatrix} = \mathcal{H}^{\dagger}\begin{bmatrix}\bar{\boldsymbol{y}}_1\\ \bar{\boldsymbol{y}}_2\end{bmatrix} &= \sqrt{\frac{\rho}{M}}\begin{bmatrix}\hat{\mathcal{H}} & \mathbf{0}_{\bar{M}}\\ \mathbf{0}_{\bar{M}} & \hat{\mathcal{H}}\end{bmatrix}\begin{bmatrix}\boldsymbol{s}_1\\ \boldsymbol{s}_2\end{bmatrix} + \mathcal{H}^{\dagger}\begin{bmatrix}\bar{\boldsymbol{z}}_1\\ \bar{\boldsymbol{z}}_2\end{bmatrix}\\ &= \sqrt{\frac{\rho}{M}}\begin{bmatrix}\hat{\mathcal{H}} & \mathbf{0}_{\bar{M}}\\ \mathbf{0}_{\bar{M}} & \hat{\mathcal{H}}\end{bmatrix}\begin{bmatrix}\boldsymbol{s}_1\\ \boldsymbol{s}_2\end{bmatrix} + \underbrace{\begin{bmatrix}\hat{\boldsymbol{z}}_1\\ \hat{\boldsymbol{z}}_2\end{bmatrix}}_{\hat{\boldsymbol{z}}}.\end{aligned} \quad (28)$$

The covariance matrix of the additive noise vector $\hat{\boldsymbol{z}}$ is

$$E[\hat{\boldsymbol{z}}\hat{\boldsymbol{z}}^{\dagger}] = \begin{bmatrix}\hat{\mathcal{H}} & \mathbf{0}_{\bar{M}}\\ \mathbf{0}_{\bar{M}} & \hat{\mathcal{H}}\end{bmatrix}.$$

Therefore, the noise vectors $\hat{\boldsymbol{z}}_1$ and $\hat{\boldsymbol{z}_s}$ are uncorrelated and have the same covariance matrix $\hat{\mathcal{H}}$. Thus, $\boldsymbol{s}_1$ and $\boldsymbol{s}_2$ can be decoded separately using $\hat{\boldsymbol{y}}_i = \hat{\mathcal{H}}\boldsymbol{s}_i + \hat{\boldsymbol{z}}_i$, $i = 1, 2$. The noise vectors $\hat{\boldsymbol{z}}_1$ and $\hat{\boldsymbol{z}_s}$ can be whitened by the same whitening matrix $\hat{\mathcal{H}}^{-1/2}$. The equivalent equations for Tx–Rx signals are

$$\hat{\mathcal{H}}^{-1/2}\hat{\boldsymbol{y}}_i = \sqrt{\rho/M}\hat{\mathcal{H}}^{1/2}\boldsymbol{s}_i + \hat{\mathcal{H}}^{-1/2}\hat{\boldsymbol{z}}_i,\quad i = 1,2. \quad (29)$$

At this point, the decoding of SAST codes becomes the detection of two groups of complex symbols $\boldsymbol{s}_i$ $(i = 1, 2)$; this is similar to the detection of 4Gp-QSTBC in (15). Our next step is to separate the real and imaginary parts of vectors $\boldsymbol{s}_i$ to obtain four groups of symbols for data detection.

Recall that $\hat{\mathcal{H}} = H_1^\dagger H_1 + H_2^\dagger H_2$, and both H_1 and H_2 are circulant. Hence, $\hat{\mathcal{H}}$ is also circulant [13]. Let $\Lambda_i = \lambda_{i,1}\ \lambda_{i,2}\ \ldots\ \lambda_{i,m}$ be the m eigenvalues of H_i $(i = 1, 2)$. We can diagonalize H_i by DFT matrix as $H_i = \mathcal{F}^\dagger \Lambda_i \mathcal{F}$. Thus, $\hat{\mathcal{H}} = \mathcal{F}^\dagger(\Lambda_1^\dagger \Lambda_1 + \Lambda_2^\dagger \Lambda_2)\mathcal{F}$. Let $\Lambda_1^\dagger \Lambda_1 + \Lambda_2^\dagger \Lambda_2 = \Lambda$, then Λ has real and non-negative entries in the main diagonal and $\hat{\mathcal{H}}^{1/2} = \mathcal{F}^\dagger \Lambda^{1/2} \mathcal{F}$ and $\hat{\mathcal{H}}^{-1/2} = \mathcal{F}^\dagger \Lambda^{-1/2} \mathcal{F}$.

We assume that $\boldsymbol{s}_i$ is premultiplied (or rotated) by an IDFT matrix $\mathcal{F}^\dagger$ of proper size. Substituting $\boldsymbol{s}_i$ by $\mathcal{F}^\dagger \boldsymbol{s}_i$ and multiplying both sides of (29) with the DFT matrix $\mathcal{F}$, we obtain

$$\begin{aligned} \Lambda^{-1/2}\mathcal{F}\hat{\boldsymbol{y}}_i &= \sqrt{\rho/M}\mathcal{F}\hat{\mathcal{H}}^{1/2}\mathcal{F}^\dagger \boldsymbol{s}_i + \Lambda^{-1/2}\mathcal{F}\hat{\boldsymbol{z}}_i \\ &= \sqrt{\rho/M}\Lambda^{1/2}\boldsymbol{s}_i + \underbrace{\Lambda^{-1/2}\mathcal{F}\hat{\boldsymbol{z}}_i}_{\tilde{\boldsymbol{z}}_i}. \end{aligned} \tag{30}$$

Since $\Lambda^{1/2}$ is a real matrix, the real and imaginary parts of $\boldsymbol{s}_i$ $(i = 1, 2)$ can now be separated for detection.

$$\Lambda^{-1/2}\Re(\mathcal{F}\hat{\boldsymbol{y}}_i) = \sqrt{\rho/M}\Lambda^{1/2}\Re(\boldsymbol{s}_i) + \Re(\tilde{\boldsymbol{z}}_i) \tag{31a}$$

$$\Lambda^{-1/2}\Im(\mathcal{F}\hat{\boldsymbol{y}}_i) = \sqrt{\rho/M}\Lambda^{1/2}\Im(\boldsymbol{s}_i) + \Im(\tilde{\boldsymbol{z}}_i). \tag{31b}$$

We finish deriving the general decoder for 4Gp-SAST codes. Using (31), one can use a sphere decoder to detect the transmitted symbols. The *equivalent channel* of 4Gp-SAST codes is $\Lambda^{1/2}$.

C. Performance Analysis

Note that the eigenvalues of $m \times m$ matrices H_1 and H_2 can be found easily using unnormalized DFT of the channel vectors $\boldsymbol{h}_1$ and $\boldsymbol{h}_2$ [13]. Therefore, the eigenvalues of H_1 and H_2 have distribution $\sim \mathcal{CN}(0, m)$.

Similar to the case of 4Gp-QSTBC, we can introduce a real orthogonal transformation R to the data vectors $\Re(\boldsymbol{s}_i)$ and $\Im(\boldsymbol{s}_i)$ $(i = 1, 2)$ to improve the performance of 4Gp-SAST codes. Thus, the actual signal rotation of 4Gp-SAST codes is $\mathcal{F}^\dagger R$.

Since the PEP of vectors $\Re(\boldsymbol{s}_i)$ and $\Im(\boldsymbol{s}_i)$ $(i = 1, 2)$ are the same, we only calculate the PEP of the vector $\Re(\boldsymbol{s}_1)$. Let $\boldsymbol{d} = \Re(\boldsymbol{s}_1)$. The PEP of distinct vectors $\boldsymbol{d}$ and $\bar{\boldsymbol{d}}$ can be calculated in a similar manner to that of 4Gp-QSTBC in Section III-C. Details are omitted for brevity. The PEP of 4Gp-SAST codes is given as

$$P(\boldsymbol{d} \to \bar{\boldsymbol{d}}) = \frac{1}{\pi}\int_0^{\pi/2}\left[\prod_{i=1}^{m}\left(1 + \frac{\rho\beta_i^2}{8\sin^2\alpha}\right)\right]^{-2} d\alpha \tag{32}$$

where $\beta_1\ \beta_2\ \ldots\ \beta_m^{\mathsf{T}} = R(\boldsymbol{d} - \bar{\boldsymbol{d}})$. One can find the asymptotic PEP of 4Gp-SAST codes at high SNR in a similar fashion to the case of 4Gp-QSTBC in (21) as follows:

$$\begin{aligned} P(\boldsymbol{d} \to \bar{\boldsymbol{d}}) &\approx \left(\frac{2^{6m}\rho^{-2m}}{\pi}\int_0^{\pi/2}(\sin\alpha)^{16}d\alpha\right)\prod_{i=1}^{m}\beta_i^{-4} \\ &= \frac{2^{6m}\rho^{-2m}}{2^{17}}\frac{16!}{8!8!}\prod_{i=1}^{m}\beta_i^{-4}. \end{aligned} \tag{33}$$

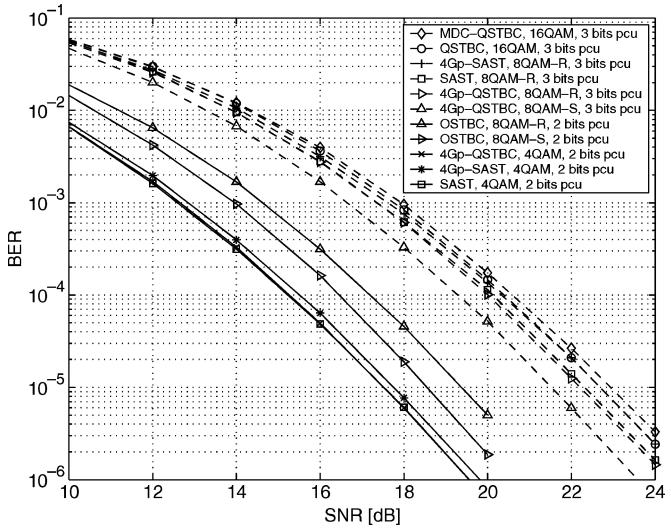

Fig. 1. Performances of 4Gp-QSTBC and 4Gp-SAST codes compared with OSTBC, MDC-QSTBC, QSTBC and SAST codes, six Tx antennas and one Rx antenna, 2 and 3 bits pcu.

Thus, if the product distance $\prod_{i=1}^{m}\beta_i$ is nonzero, 4Gp-SAST codes will achieve full-diversity. Similar to 4Gp-QSTBC, with QAM, the signal rotations R_{BOV} in [21] and [22] can be used to minimize the worst-case PEP.

Remark: It is interesting to recognize that, the optimal rotation matrices of 4Gp-QSTBC $(R = \Theta R_{BOV})$ and 4Gp-SAST codes $(R = \mathcal{F}R_{BOV})$ have a similar formula. The precoding matrices Θ and $\mathcal{F}$ are added to diagonalize the channels of the two codes. Thus, each real symbol is equivalently transmitted in a separate channel, but full diversity is not achievable. The real rotation matrix R_{BOV} is applied to the data vectors so that the real symbols are spread over all the channels, and thus full diversity is achievable.

V. Simulation Results

Simulation results are presented in Fig. 1 to compare the performances of 4Gp-QSTBC and 4Gp-SAST codes with OSTBC, MDC-QSTBC [12], QSTBC [6], and SAST codes [10] for six Tx and one Rx antennas. To produce the desired bit rates, two 8QAM constellations are used. The first constellation is rectangular, denoted by 8QAM-R, and has signal points $\{\pm 1 \pm \mathrm{j}, \pm 3 \pm \mathrm{j}\}$. The other constellation, denoted by 8QAM-S, has the best minimum Euclidean distance; its geometrical shape is depicted in [6, Fig. (2c)].

We compare the performance of our new codes with OSTBC and SAST codes for a spectral efficiency of 2 bits pcu. To get this bit rate, 8QAM signals are combined with rate-2/3 OSTBC, while 4QAM is used for the SAST, 4Gp-QSTBC, and 4Gp-SAST codes. Two columns (4 and 8) of 4Gp-QSTBC for eight Tx antennas are deleted to create the code for six Tx antennas. From Fig. 1, 4Gp-SAST codes gains 0.8 and 1.6 dB over OSTBC with 8QAM-S and 8QAM-R, respectively, while the decoding complexity slightly increases (see Table I). The performance improvement of 4Gp-QSTBC is even better: 1 dB compared with OSTBC (using 8QAM-S) and 0.2 dB compared with 4Gp-SAST codes. Note that for six antennas, the decoding complexity of 4Gp-QSTBC is slightly higher than that of 4Gp-SAST codes (see Table I).

In Fig. 1, the performance of 4Gp-QSTBC and 4Gp-SAST codes with 3 bits pcu is also compared with that of the rate-3/4 QSTBC and MDC-QSTBC (using 16QAM). 4Gp-SAST code yields a 0.3 dB improvement over MDC-QSTBC and performs the same as QSTBC.

Specifically, 4Gp-QSTBC using 8QAM-S performs much better than the QSTBC; it produces a 1.2 dB gain over QSTBC with the same decoding complexity.

Further simulations for five and eight Tx antennas also confirm that 4Gp-QSTBC and 4Gp-SAST codes perform better than OSTBC, MDC-QSTBC, QSTBC, and SAST codes. Due to the lack of space, we omit the details.

VI. Conclusion

We have presented two new rate-one STBC with four-group decoding, called 4Gp-QSTBC and 4Gp-SAST codes. They offer the lowest decoding complexity compared with the existing rate-one STBC. Their closed-form PEP are derived, enabling the optimization of signal rotations. Compared with other existing low decoding complexity STBC (such as OSTBC, MDC-QSTBC, CIOD, and QSTBC), our newly designed STBC have several additional advantages including higher code rate, better BER performance, lower encoding/decoding delay, and lower peak-to-average power ratio (PAPR) because zero-amplitude symbols are avoided in the code matrices. Recent results in [23] present a flexible design of multigroup STBC. However, the code rate is still limited by 1 symbol pcu. Thus, the systematic design of a high-rate multigroup STBC is still an open research problem.

Acknowledgment

The authors would like to thank the anonymous reviewers for their constructive comments, which greatly improved the presentation of the paper.

References

[1] S. M. Alamouti, "A simple transmitter diversity scheme for wireless communication," *IEEE J. Sel. Areas Commun.*, vol. 16, pp. 1451–1458, Oct. 1998.

[2] V. Tarokh, H. Jafarkhani, and A. R. Calderbank, "Space–time block codes from orthogonal designs," *IEEE Trans. Inf. Theory*, vol. 45, no. 5, pp. 1456–1466, Jul. 1999.

[3] X.-B. Liang, "Orthogonal designs with maximal rates," *IEEE Trans. Inf. Theory*, vol. 49, no. 10, pp. 2468–2503, Oct. 2003.

[4] H. Jafarkhani, "A quasi-orthogonal space–time block code," *IEEE Trans. Commun.*, vol. 49, no. 1, pp. 1–4, Jan. 2001.

[5] O. Tirkkonen, A. Boariu, and A. Hottinen, "Minimal nonorthogonality rate 1 space–time block code for 3+ Tx antennas," in *Proc. IEEE 6th Int. Symp. Spread-Spectrum Techniques Applications (ISSSTA 2000)*, Parsippany, NJ, Sep. 2000, pp. 429–432.

[6] W. Su and X.-G. Xia, "Signal constellations for quasi-orthogonal space–time block codes with full diversity," *IEEE Trans. Inf. Theory*, vol. 50, no. 10, pp. 2331–2347, Oct. 2004.

[7] B. Badic, H. Weinrichter, and M. Rupp, "Comparison of non-orthogonal space–time block codes in correlated channels," in *Proc. IEEE Workshop Signal Processing Advances in Wireless Communications (SPAWC)*, Lisbon, Portugal, Jul. 2004, pp. 268–272.

[8] N. Sharma and C. B. Papadias, "Full-rate full-diversity linear quasi-orthogonal space–time codes for any number of transmit antennas," *EURASIP J. Appl. Signal Process.*, vol. 9, pp. 1246–1256, Aug. 2004.

[9] A. Sezgin and T. J. Oechtering, "On the outage probability of quasi-orthogonal space–time codes," in *Proc. IEEE Inf. Theory Workshop (ITW)*, San Antonio, TX, Oct. 2004, pp. 381–386.

[10] D. N. Dào and C. Tellambura, "Capacity-approaching semi-orthogonal space–time block codes," presented at the IEEE GLOBECOM, St. Louis, MO, Nov./Dec. 2005.

[11] M. O. Damen, H. El Gamal, and G. Caire, "On maximum-likelihood detection and the search for the closest lattice point," *IEEE Trans. Inf. Theory*, vol. 49, no. 10, pp. 2389–2402, Oct. 2003.

[12] C. Yuen, Y. L. Guan, and T. T. Tjhung, "Quasi-orthogonal STBC with minimum decoding complexity," *IEEE Trans. Wireless Commun.*, vol. 4, no. 5, pp. 2089–2094, Sep. 2005.

[13] P. J. Davis, *Circulant Matrices*, 1st ed. New York: Wiley, 1979.

[14] B. Hassibi and B. M. Hochwald, "High-rate codes that are linear in space and time," *IEEE Trans. Inf. Theory*, vol. 48, no. 7, pp. 1804–1824, Jul. 2002.

[15] V. Tarokh, N. Seshadri, and A. R. Calderbank, "Space–time codes for high data rate wireless communication: Performance analysis and code construction," *IEEE Trans. Inf. Theory*, vol. 44, pp. 744–765, Mar. 1998.

[16] C. Yuen, Y. L. Guan, and T. T. Tjhung, "On the search for high-rate quasi-orthogonal space–time block code," *Int. J. Wireless Information Network (IJWIN)*, vol. 13, pp. 329–340, Oct. 2006.

[17] M. Z. A. Khan and B. S. Rajan, "Single-symbol maximum likelihood decodable linear STBCs," *IEEE Trans. Inf. Theory*, vol. 52, no. 5, pp. 2062–2091, May 2006.

[18] C. Yuen, Y. L. Guan, and T. T. Tjhung, "A class of four-group quasi-orthogonal space–time block code achieving full rate and full diversity for any number of antennas," in *Proc. IEEE Personal, Indoor, Mobile Radio Communications Symp. (PIMRC)*, Berlin, Germany, Sep. 2005, pp. 92–96.

[19] M. K. Simon and M.-S. Alouini, *Digital Communication Over Fading Channels*, 1st ed. New York: Wiley, 2000.

[20] J. W. Craig, "A new, simple and exact result for calculating the probability of error for two-dimensional signal constellations," in *Proc. IEEE Military Communications Conf. (MILCOM)*, Boston, Nov. 1991, pp. 25.5.1–25.5.5.

[21] E. Bayer-Fluckiger, F. Oggier, and E. Viterbo, "New algebraic constructions of rotated Z^n-lattice constellations for the Rayleigh fading channel," *IEEE Trans. Inf. Theory*, vol. 50, no. 4, pp. 702–714, Apr. 2004.

[22] F. Oggier and E. Viterbo, Full Diversity Rotations [Online]. Available: www1.tlc.polito.it/~viterbo/rotations/rotations.html.

[23] S. Karmakar and B. S. Rajan, "Multi-group decodable STBCs from clifford algebras," in *Proc. IEEE Inf. Theory Workshop (ITW)*, Chengdu, China, Oct. 2006, pp. 448–452.

[24] H. Kan and H. Shen, "A counterexample for the open problem on the minimal delays of orthogonal designs with maximal rates," *IEEE Trans. Inf. Theory*, vol. 51, no. 1, pp. 355–359, Jan. 2005.